

Abnormal focal length increase of terajet generated in reflection mode

Yu-Jing Yang(杨育静), Jiang-Tao Qin(秦江涛), De-Long Zhang(张德龙), Sai-Dong Xue(薛赛东), and Ning Yuan(袁宁)

Citation: Chin. Phys. B, 2025, 34 (**9**): 094204. DOI: 10.1088/1674-1056/add903
http://cpb.iphy.ac.cn; http://iopscience.iop.org/cpb

What follows is a list of articles you may be interested in

All-chalcogenide glass based high fill-factor long-wave infrared micro-metalens array with superior optical flexibility

Zhaofeng Gu(谷招峰), Kongsi Zhou(周孔思), Tong Sun(孙童), Yixiao Gao(高一骁), Yimin Chen(陈益敏), Zijun Liu(刘自军), Chenjie Gu(顾辰杰), Pengfei Lu(芦鹏飞), and Xiang Shen(沈祥)

Chin. Phys. B, 2025, 34 (**7**): 074213. DOI: 10.1088/1674-1056/add4f5

High-power xenon lamp-pumped Er:YAP pulse laser operated in free-running and acousto-optical *Q*-switching modes

Cong Quan(权聪), Dunlu Sun(孙敦陆), Huili Zhang(张会丽), Jianqiao Luo(罗建乔), Zhiyuan Han(韩志远), Yang Qiao(乔阳), Yuwei Chen(陈玮威), Zhentao Wang(王镇涛), Maojie Cheng(程毛杰), and Qingli Zhang(张庆礼)

Chin. Phys. B, 2023, 32 (**11**): 114207. DOI: 10.1088/1674-1056/ace8f7

Microwave absorption and bandwidth study of Y_2Co_{17} rare earth soft magnetic alloy with easy-plane anisotropy

Yun-Guo Ma(马云国), Liang Qiao(乔亮), Zu-Ying Zheng(郑祖应), Hong-Bo Hao(郝宏波), Hao Wang(王浩), Zhe Sun(孙哲), Cheng-Fa Tu(涂成发), Tao Wang(王涛), Zheng Yang(杨正), and Fa-Shen Li(李发伸)

Chin. Phys. B, 2023, 32 (**8**): 084202. DOI: 10.1088/1674-1056/aca148

Design of an all-dielectric long-wave infrared wide-angle metalens

Ning Zhang(张宁), Qingzhi Li(李青芝), Jun Chen(陈骏), Feng Tang(唐烽),Jingjun Wu(伍景军), Xin Ye(叶鑫), and Liming Yang(杨李茗)

Chin. Phys. B, 2022, 31 (**7**): 074212. DOI: 10.1088/1674-1056/ac4026

Large aperture phase-coded diffractive lens for achromatic and 16° field-of-view imaging with high efficiency

Gu Ma(马顾), Peng-Lei Zheng(郑鹏磊), Zheng-Wen Hu(胡正文), Suo-Dong Ma(马锁冬), Feng Xu(许峰), Dong-Lin Pu(浦东林), and Qin-Hua Wang(王钦华)

Chin. Phys. B, 2022, 31 (**7**): 074210. DOI: 10.1088/1674-1056/ac560c

---

Abnormal focal length increase of terajet generated in reflection mode

Yu-Jing Yang(杨育静)[1], Jiang-Tao Qin(秦江涛)[1], De-Long Zhang(张德龙)[1,†], Sai-Dong Xue(薛赛东)[2,‡], and Ning Yuan(袁宁)[3,§]

[1] *Department of Opto-electronics and Information Engineering, School of Precision Instruments and Opto-Electronics Engineering, Key Laboratory of Optoelectronic Information Technology (Ministry of Education), and Key Laboratory of Micro-Opto-Electro-Mechanical Systems (MOEMS) Technology (Ministry of Education), Tianjin University, Tianjin* 300072, *China*

[2] *College of Electrical and Electronic Engineering, Anhui Science and Technology University, Bengbu* 233030, *China*

[3] *Tianjin Sino–German University of Applied Sciences, Tianjin* 300350, *China*

(Received 3 March 2025; revised manuscript received 2 May 2025; accepted manuscript online 15 May 2025)

We report an interesting and abnormal electromagnetic phenomenon with regard to a terajet (TJ) that is generated in a reflection mode, which is realized by placing a dielectric scatterer onto a metal reflection plate. We show that the introduction of an air hollow into metal reflection plate beneath the scatterer does not induce an expected decrease but an abnormal increase of focal length of the TJ by as much as more than three times. This abnormal phenomenon takes place in case that the air hollow is shallow and there exists a critical hollow depth for a given lateral size of air hollow. Larger than the critical depth, the phenomenon no longer occurs. It is explained from viewpoints of both ray optics in terms of role of relative portion of central waves in TJ formation and electromagnetic field theory with regard to hollow-induced phase singularities.

Keywords: terajet, reflection mode, air hollow, focal length, phase singularity

PACS: 42.25.Bs, 42.25.Fx, 42.50.St, 42.25.Hz

DOI: 10.1088/1674-1056/add903 **CSTR:** 32038.14.CPB.add903

1. Introduction

Photonic jet/terajet (PJ/TJ) is a highly focused light/terahertz wave beam featured by high intensity, narrow beam waist, wavelength-scale propagation distance and weak diffraction.[1–3] Three parameters, including wave intensity enhancement factor, focal length (FL), and FWHM (full-width at half maximum) at focal position, are usually used to characterize it. Among them, the FL determines the application scenarios of the PJ/TJ jet.[4–6] The PJ/TJ in a transmission mode always generated by a wavelength-sized particle under the illumination of incident wave. And the formation of PJ/TJ can be regarded as the interference of incident waves and the waves scattered by the microparticle. On the other hand, the PJ/TJ generation can be also interpreted in light of geometric optics, *i.e.*, it can be thought as the focusing of the lights by the microparticle, and the microparticle functions as a microlens. In this sense, some viewpoints in geometric optics can be used to quantitatively explain the features of PT/TJ.[7]

As an alternative, a PJ/TJ can be also generated in a reflection mode,[8–16] which is usually realized by putting a dielectric scatterer onto a mirror, such as a high-refractive-index plate or a metallic thin-film coated onto a substrate. For a PJ/TJ generated in the reflection mode, its FL can be effectively tailored by either changing the geometry of scatterer[8] or changing the refractive index of the reflective plate,[11] or adding a metal mask onto the dielectric scatterer,[13] and or introducing an air hollow into the reflection plate.[14,15] A PJ/TJ produced in the reflection mode has great potential in applications of optical trapping of nanoparticles,[9,10] biomedical sampling in liquid,[11] development of flat focusing mirror,[12] collection and enhancement of Raman scattering and photoluminescence signals,[17–19] as well as stability improvement of nanoparticles' Brownian motion.[20]

The abnormal optical phenomenon reported here is related to a TJ generated in a reflection mode, which is realized by putting a mesoscale dielectric scatterer onto a metallic reflection plate under illumination of an incident plane terahertz wave. As demonstrated later, the introduction of an air hollow into metal reflection plate beneath the scatterer induces an increase of TJ's FL by as much as several times in case that the air hollow is shallow. Such a TJ characteristic is abnormal as a reversed feature that the air hollow induces the FL decrease is expected in point of view of ray optics instead. In this paper, we demonstrate this interesting and abnormal electromagnetic phenomenon. It is qualitatively interpreted in lights of ray optics and electromagnetic field theory.

†Corresponding author. E-mail: dlzhang@tju.edu.cn

‡Corresponding author. E-mail: xuesaidong@hotmail.com

§Corresponding author. E-mail: yuanning0321@163.com

© 2025 Chinese Physical Society and IOP Publishing Ltd. All rights, including for text and data mining, AI training, and similar technologies, are reserved.

It is worthwhile to point out that in our previous papers we have carried out numerical studies on the characteristics of the TJs generated in the reflection mode.[13–15] These studies focused on the TJ shaping realized by making use of different methods such as the one of putting a metal mask onto the dielectric scatterer,[13] the ones of introducing a penetrated[14] or unpenetrated air hollow[15] into the reflection plate (the studies showed that the shaping characteristics in two cases of perforative and not perforative air hollows are quite different because of different shaping mechanisms). In addition, based on TJs generated in the reflection mode we have demonstrated a large-range refractive sensor.[16] In particular, the phenomenon that in some special conditions, the TJ generated in case of an air hollow being introduced into the metal reflection plate has the larger FL than that of the TJ generated without hollow has been firstly observed in our previous work.[14] However, these previous works neither identify the phenomenon as "abnormal" one, none carry out a systematic or in-depth study on the abnormal phenomenon reported in present work. This paper aims to explore the conditions, physical principles, and potential application of this abnormal phenomenon.

2. Structure model and numerical method

Figure 1(a) shows the schematic of a TJ generated in a reflection mode. The scattering system consists of a cuboid dielectric scatterer and a metallic reflection plate, in which an air hollow is embedded and located beneath the scatterer. A Cartesian coordinate system is fixed at the center of the top surface of the scatterer. Figures 1(b) and 1(c) show the projections of scatterer structure onto xz (yz) and xy planes, respectively. The scatterer, reflection plate and air hollow all have a square bottom surface (on xy plane) with a side length of L, $L_{\rm rp}$, and $L_{\rm hol}$ in order, and a height/depth along z-axis of H, $H_{\rm rp}$, and $D_{\rm hol}$, respectively, among which the scatterer geometry is taken from Ref. [7], together with the materials designed for the scatterer and reflection plate. The scatterer adopts the Teflon material, which has a refractive index 1.46 at the studied wavelength $\lambda = 3$ mm.[21] The reflection plate is an aluminum metallic material with an electric conductivity 3.56×10^7 S/m. The air hollow is indicated by red dashed lines in Figs. 1(b) and 1(c). All the centers of scatterer, reflection plate, and hollow are located on the z axis.

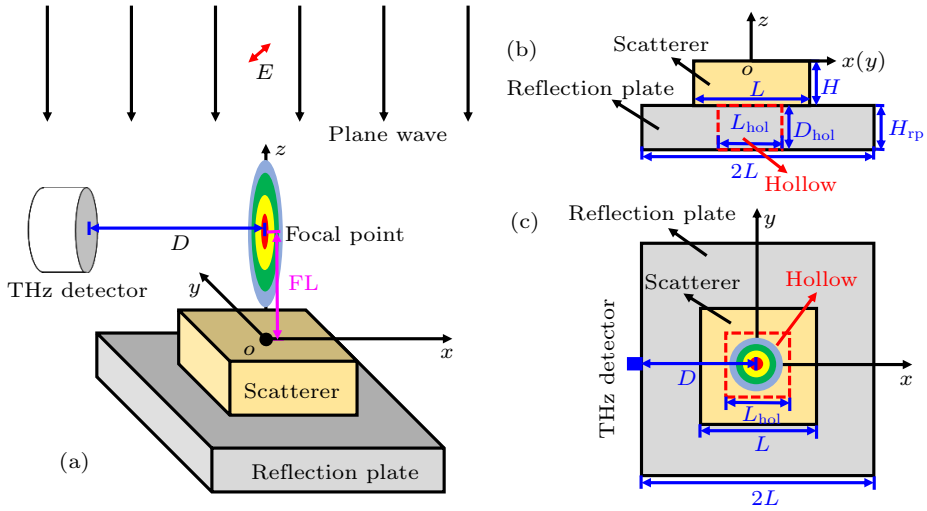


Fig. 1. (a) Schematic diagram of TJ generated in reflection mode realized by a scattering system consisted of a dielectric scatterer and a reflection plate with an air hollow embedded in it. Projections of scattering structure onto (b) xz or yz and (c) xy planes.

A plane terahertz wave polarized along the diagonal line of xy plane is incident onto the scattering system along the negative z-axis. The incident wave with a wavelength λ and an intensity I_0 is firstly scattered by the dielectric scatterer, and then reflected by the reflection plate. At last, the reflected waves and scattered waves interfere with incident waves in $z > 0$ space, resulting in formation of a TJ as shown in Fig. 1(a), where the TJ projected onto the xz plane is given. The magenta arrow indicates the TJ's FL, defined as the distance along z-axis from top surface of scatterer to the z position where the intensity maximizes, *i.e.*, the focal point indicated in Fig. 1(a). Aiming at the scattering system depicted in Fig. 1(a), we have done a simulation on the TJ characteristics.

The numerical simulation was performed by aid of a commercially available program (CST Microwave Studio) based on a finite integration method. A transient solver in time domain was used. The open boundary conditions, which is usually used to calculate scattered fields, were set in three directions. It means that the surrounding medium is an infinite air space without reflection. To guarantee calculation accuracy, a sufficiently fine hexahedral mesh with a size of $\lambda/60$ was adopted for the whole computational domain, and an adaptive mesh refinement and a strict iterative termination condition have been also adopted. In the simulation, the scatterer

has a fixed geometry of $L = \lambda$ and $H = 0.33\lambda$ while the air hollow has a varied geometry of $L_{\rm hol}$ and $D_{\rm hol}(= H_{\rm rp})$ to shape the TJ generated.

3. Results and discussion

Figure 2 shows the projected TJs generated by the scattering system without a hollow [panel (a)] and with a hollow ($D_{\rm hol} = 0.1H$ and $W_{\rm hol} = 0.5\lambda$) [panel (b)]. The white dashed line marks the focal position. Some background spots are observed in Figs. 2(a) and 2(b). They are formed by some standing waves generated by interference of reflected and incident waves, and are usually observed in a reflection mode.[8,9,11] These noise spots affect definitely the TJ generation.

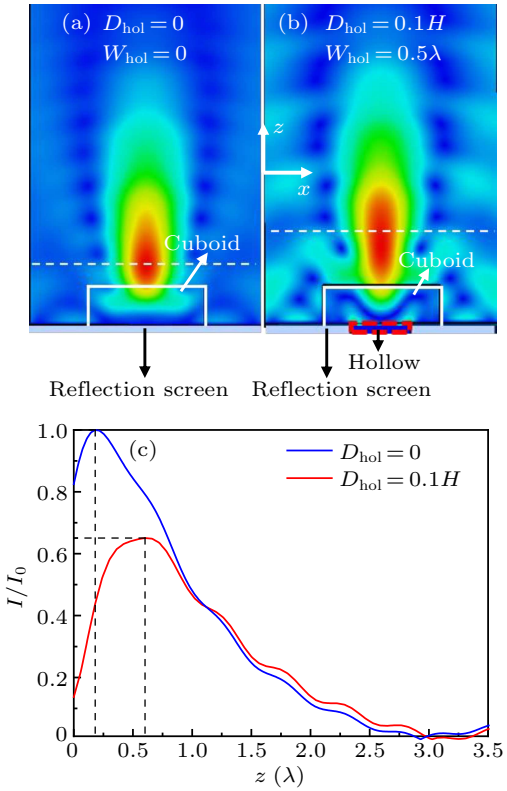


Fig. 2. Projected patterns of the TJs generated by the scattering system (a) without a hollow, (b) with a hollow having $D_{\rm hol} = H_{\rm rp} = 0.1H = 0.033\lambda$ and $W_{\rm hol} = 0.5\lambda$. (c) Wave intensity distributions (along z-axis) of the TJs involved in (a) and (b).

It is evident that the focal position of TJ moves away from the reflection plate as one goes from Fig. 2(a) to Fig. 2(b). The feature suggests that the introduction of an air hollow into metal reflection plate induces a considerable increase of TJ's FL. To further quantify the increase, in Fig. 2(c) we comparatively show the normalized wave intensity (I/I_0) distributions (along z-axis) of two TJs generated in the two cases without ($D_{\rm hol} = 0$) and with the air hollow ($D_{\rm hol} = 0.1H$). The vertical dashed lines mark the focal positions. From the focal positions, we can obtain the TJ's FL value. It is similar to 0.18λ in the case without the air hollow, while increases to 0.59λ as an air hollow is introduced. One can see that the increase is as much as ~ 3.3 times.

The phenomenon that the introduction of an air hollow into metal reflection plate induces a significant FL increase is abnormal in light of ray optics as stated below. According to the Fermat principle, only rays with the same optical path could be focused onto an identical point, *i.e.*, the focal point. As we know, the scattered waves have a definite extent of angular profile. In case that the air hollow is present in the reflection plate, some waves scattered by the cuboid enter into the air hollow and part of them are reflected by the metallic walls of the hollow. Because these reflected waves have additional optical paths inside the hollow, they need propagate shorter distances to match with the optical paths of either those reflected scattered waves without entering into the hollow or the reflected waves without experiencing the scattering. The TJ should therefore have a shorter FL in comparison with the case without the air hollow introduced. Without the air hollow, all of the scattered waves are reflected directly. They need propagate longer distances to match with the optical paths of the reflected waves without experiencing the scattering. As a result, a TJ with a longer FL is generated. In words, in light of ray optics, the introduction of the air hollow should induce an FL decrease. This is contradictory to the observed feature as described above. The feature that the introduction of an air hollow induces an FL increase is thus abnormal. This abnormal phenomenon may be further understood from the viewpoint of ray optics in terms of role of relative portion of central waves in the TJ formation as detailed below. Consider that the incident waves are divided into two parts: central and edge waves. The central waves are defined as the ones incident onto the scatterer and the edge waves are defined as those directly incident onto the reflection plate. In case that the hollow is absent, the central waves returning to $z > 0$ zone have larger optical path and more advanced optical phase than those edge waves because the central waves pass through twice the dielectric scatterer while the edge waves propagate always in the air medium before and after the reflection. To match with the optical phase of the edge waves so as to realize a constructive interference, the central waves need propagate a shorter distance. As a result, a TJ with a smaller FL is generated. This means that the central waves play a predominant role in formation of a TJ having a smaller FL.

When an air hollow is introduced into the reflection plate, partial central waves leak out of the system. The leakage leads to the reduction of relative portion of the central waves participated in the interference and TJ formation. As a result, the central waves in this case play a minor role in the TJ formation. It is thus comprehensible that the introduction of air hollow leads to the FL increase of the TJ. This point is clearly shown in Fig. 2. The argument that the reduction of the relative portion of central waves leads to the TJ's FL increase is further supported by additional simulation results given by changing

the reflection plate size $L_{\rm rp}$ while keeping the hollow size unchanged, which gives rise to the change of relative portion of central waves. Figure 3 shows the simulated dependence of TJ's FL on the reflection plate side length $L_{\rm rp}$ in case that the hollow geometry is fixed at $L_{\rm hol} = 0.5\lambda$ and $D_{\rm hol} = 0.1H$. As expected, the FL increases significantly with the increase of the $L_{\rm rp}$. This is ascribed to the increase of relative portion of edge waves, *i.e.*, the corresponding reduction of relative portion of central waves.

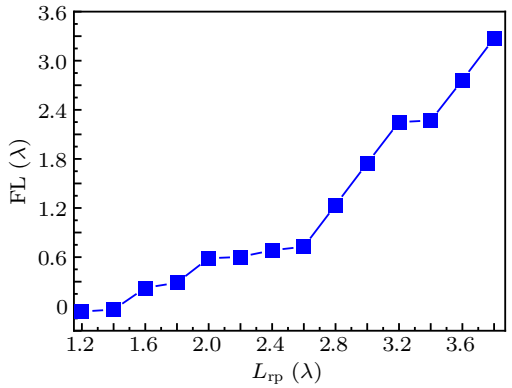


Fig. 3. Reflection plate side length $L_{\rm rp}$ dependence of TJ's FL in case that the hollow geometry is fixed at $L_{\rm hol} = 0.5\lambda$ and $D_{\rm hol} = 0.1H$.

The abnormal phenomenon can be also qualitatively explained from point of view of electromagnetic field theory in respect to hollow-induced number and position changes of phase singularities in the Poynting vector distribution of TJ. Figure 4 shows two-dimensional (2D) Poynting vector distributions (on *xz* plane) of scattered waves inside and outside the scatterer for the TJs generated in cases of fixed hollow width $W_{\rm hol}$ of 0.5λ and varied $D_{\rm hol}$. Figures 4(a)–4(d) correspond to the cases of $D_{\rm hol}$ from 0, $0.1H$, $0.4H$, and $1.4H$, respectively. Because the Poynting vector distributions inside the dielectric scatterer change significantly due to the introduction of air hollow, only the distributions there and those in its adjacent regions are shown. The color of Poynting vector reflects the wave intensity and the tiny arrows indicate the power flow directions. The large, thick red arrow indicates the general direction of power flow there.

The attention is firstly paid to the direction of power flow. As indicated by thick red arrows in Fig. 4(a), all the central waves are firstly scattered by the cuboid, and then reflected by the reflection plate, and scattered by the cuboid again prior to returning to the $z > 0$ space. As for the edge waves, some of them directly return to the space $z > 0$ without interacting with the scatterer after being reflected by the plate, others are firstly reflected by the reflection plate and then flow into the central region to interact with the scatterer, prior to returning to the $z > 0$ space. However, in Figs. 4(b)–4(d), the waves behave differently. For the wave incident onto the scatterer, some of them leak into the hollow without experiencing a reflection, others are still scattered by the cuboid before being reflected by the reflection plate, and then scattered again prior to returning to the $z > 0$ space. For the edge waves, majority of them flow into the central region to interact with the scatterer before leaking into the hollow.

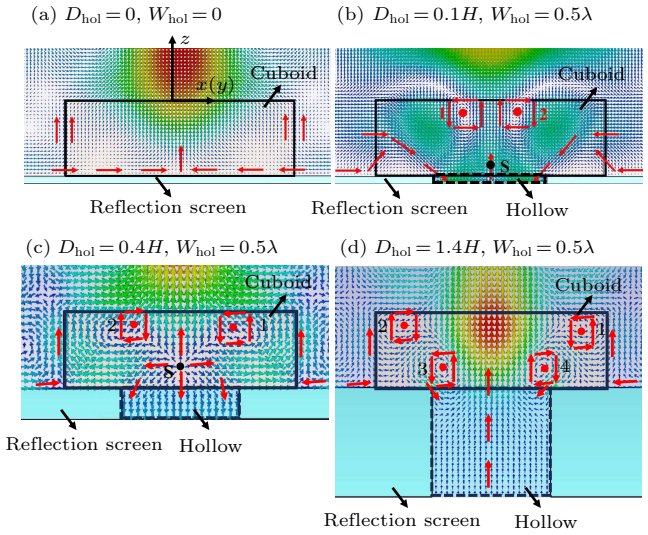


Fig. 4. The 2D Poynting vector distributions of scattered waves inside and outside the scatterer for the TJs generated in cases of $W_{\rm hol} = 0.5\lambda$, and $D_{\rm hol} = 0$ (a), $0.1H$ (b), $0.4H$ (c), and $1.4H$ (d).

Attention is next paid to phase singularity in the electromagnetic field distribution of TJs. The optical vortex and saddle point are two typical types of phase singularities. The former usually appears as a vortex around which the power flows end to end, and the latter can be recognized by the radial power flow direction. It is known that the direction of Poynting vector represents the direction of energy flow in the region. To intuitively show the dependence of the phase singularities in the TJ distribution on the hollow geometry, figure 4 show the Poynting vector distribution of TJs generated in different cases. In Fig. 4(a), no phase singularity is observed. However, in Figs. 4(b)–4(c), there are two vortex phase singularities marked with red dots and red numbers and one saddle phase singularity marked with "S". The power flow around each vortex singularity forms a counterclockwise 1 or clockwise 2 wave vortexes as indicated by red arrows end-to-end. As two power flow vortices have the opposite rotation directions, a saddle phase singularity is generated there, around which the power hyperbolically flows away. The generation of phase singularity is closely related to the energy exchange that takes place in the near region.[22,23] In comparison, one can see that in Figs. 4(b)–4(c), the wave vortexes and saddle phase singularities have the equal numbers but different positions. In fact, both the TJs in Figs. 4(b)–4(c) have the FL larger than that of TJ in Fig. 4(a) without air hollow. This means that the discussed abnormal phenomenon is closely related to the number of phase singularities in Poynting vector distribution of TJs. Moreover, the positions of phase singularities in two cases are different, and thereby the TJs in Figs. 4(b) and 4(c)

have the different FL value. In Fig. 4(d), there are four wave vortexes inside the scatterer. Similarly, the power flows rotating counterclockwise form the vortex singularities 1 and 3, while the ones rotating clockwise form the vortex singularities 2 and 4. The completely different phase singularities cause the TJ generated in this case has an FL smaller than that of the TJ generated without air hollow.

In words, the introduction of an air hollow into reflection plate results in remarkable changes of power flow direction and hence the generation of some phase singularities, which dramatically affect the circulation of power flow and the exchange of electromagnetic energy in related regions. As a result, the interference pattern and hence the characteristic parameters of TJ change substantially and possibly unusually. This is the reason why the introduction of an air hollow induces an abnormal FL increase. In addition, the number and positions of phase singularities affect the FL of TJs generated, and hence are closely related to the abnormal phenomenon.

Further study shows that the abnormal phenomenon is only observed in some specific cases in respect to hollow geometry. Figure 5(a) shows air hollow depth $D_{\rm hol}$ dependences of TJ's FL for different hollow side lengths of $L_{\rm hol} = 0.4\lambda$, 0.5λ, 0.6λ, and 0.7λ. A varying range of $D_{\rm hol}$ from $0.0H$ to $1.4H$ is considered here. The black, red, blue, and magenta lines represent the cases of $L_{\rm hol} = 0.4\lambda$, 0.5λ, 0.6λ, and 0.7λ, respectively. We first note that the FL shows considerable hollow depth $D_{\rm hol}$ and side length $L_{\rm hol}$ effects. As the $D_{\rm hol}$ is increased, the FL decreases remarkably. This is expected in light of ray optics. The effect is related to the reflection of the scattered waves by the metallic walls of the hollow. When the hollow has a smaller depth, the scattered waves are reflected fewer times by the hollow walls. These reflected waves have shorter optical paths inside the hollow and need propagate a longer distance to match with the optical path of those scattered waves without entering the hollow. As a result, the generated TJ has a longer FL. In case that the hollow has a larger depth, the scattered waves are reflected more times by the hollow walls. These reflected waves have longer optical paths inside the hollow, they need to propagate a shorter distance to match with the optical path of those scattered waves without entering the hollow. As a result, the generated TJ has a shorter FL. Different from the $D_{\rm hol}$ effect, the $L_{\rm hol}$ effect is not so regular. The change of FL with $L_{\rm hol}$ shows non-monotonous varying feature.

Subsequently, we turn to discuss with an emphasis on the occurrence condition of the abnormal phenomenon. Based on the preceding results and discussion, the FL value (0.18λ) of the TJ generated in the case without an air hollow introduced can be regarded as the criterion for the occurrence of the abnormal phenomenon. For convenience, it is marked in Fig. 5 by a horizontal dotted line. When FL $> 0.18\lambda$, the abnormal phenomenon takes place. Smaller than 0.18λ, such FL value is normal. Based on this criterion, from Fig. 5(a) we can discriminate the specific hollow geometries that the abnormal phenomenon occurs. It is evident that the occurrence of the abnormal phenomenon depends on both $D_{\rm hol}$ and $L_{\rm hol}$. For a given $L_{\rm hol}$, there exists a critical $D_{\rm hol}$ value. Smaller than the critical value, the abnormal phenomenon takes place. Larger than the critical value, the abnormal phenomenon no longer occurs. The critical $D_{\rm hol}$ value changes with the $L_{\rm hol}$. In words, the abnormal phenomenon takes place in case that the air hollow is shallow and there exists a critical hollow depth for a given hollow width.

As we know, a PJ/TJ is featured by a sub-wavelength scaled full-width at half maximum (FWHM), defined as the FWHM of the intensity profile along the x-/y-axis at the focal point. A PJ/TJ with an FWHM larger than $> \lambda$ is no longer a strict PJ/TJ. It is therefore essential to simultaneously consider the FL and the FWHM. Figure 5(b) shows the $D_{\rm hol}$ dependences of the FWHM of the TJs generated in the cases same as Fig. 5(a). We can see that the FWHM shows a decreasing tendency with the increase of $D_{\rm hol}$. As the $D_{\rm hol}$ is increased from $0.1H$ to $1.4H$, the FWHM decreases from 0.55λ to 0.25λ. The decrease of FWHM with the $D_{\rm hol}$ matches with the decrease of FL with the $D_{\rm hol}$. As the FL is decreased, the TJ beam becomes more compact[14] and hence has a smaller FWHM value. We note that the FWHM values of the TJs here keep always at the sub-wavelength scale in the studied $D_{\rm hol}$ range of $0.1H$–$1.4H$ and $L_{\rm hol}$ range of 0.4λ–0.7λ, implying that all of the beams concerned remain still the TJ feature.

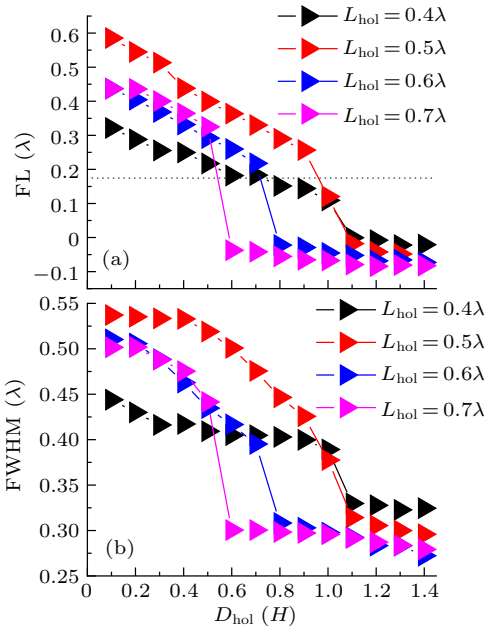


Fig. 5. Air hollow depth $D_{\rm hol}$ dependence of TJ's (a) FL and (b) FWHM for different hollow side lengths of $L_{\rm hol} = 0.4\lambda$, 0.5λ, 0.6λ, and 0.7λ. The horizontal dotted line marks the FL value (0.18λ) of the TJ generated in the case without an air hollow introduced.

The significant FL increase facilitates the practical applications of the TJ. A TJ with longer FL may find its use in

many fields, such as (i) manipulation and detection of single nanoparticle and biomolecule, (ii) control of on/off of an optical path, (iii) color splitter of dielectric double-material for image sensor, (iv) measurement of rotation speed for a motor, (v) non-destructive metrology for semiconductor devices, (vi) imaging of reflective fluorescence/confocal microscopy, (vii) power enhancement of antennas radiation, and (viii) on-chip bendable wave communications. In specific, for the nanomanipulation and detection, the TJ beam acts as an operating arm, and the TJ with a longer FL means an optical-tweezer with the longer arm and can work in a larger space; for the control of optical switch, the TJ with a longer FL corresponds to a larger working distance; and for the on-chip communications, the TJ with a longer FL ensures a longer signal transmission distance.

Finally, it is essential to suggest an experimental scheme for the measurements of TJ performance parameters, including the FL and FWHM. Here, we propose a possible one. That is to measure the TJ beam projected onto the *xz* or *yz* plane. This can be done by using a terahertz wave detector to take a picture of the TJ beam. If the picture is taken along with the optical axis *z*, there exists two problems to be overcome. First, in this case the detector must be arranged in a position between the wave source and the scatterer. It inevitably blocks incident waves and hence affects the TJ formation. Second, for this detection configuration, the TJ projected onto the *xy* plane is measured. To get the values of FL and FWHM parameters (at focal point), one must fix the focal point. To avoid these two problems, here we propose to take the picture along with the direction parallel to the *x* or *y* axis as shown in Fig. 1(a). To avoid the issue of blocking the incident wave, one needs to fix the detector to the edge of the reflection plate as indicated in Figs. 1(a) and 1(c). Due to the distance between the center and edge of the reflection plate D is just one wavelength and the distance between the detector and the detected TJ beam is smaller than one wavelength, there is no need to use a terahertz imaging lens to help to collect waves. From the captured image, one can obtain 2D TJ intensity distributions on the *xz* or *yz* plane. From the spatial distributions, one can further obtain the FL and FWHM parameters.

4. Conclusion

In conclusion, we have demonstrated an abnormal electromagnetic phenomenon that the introduction of air hollow into reflection plate results in an FL increase by more than three times. The abnormal feature can be explained from viewpoints of both ray optics in terms of role of relative portion of central waves in TJ formation and electromagnetic field theory in respect to hollow-induced phase singularities in the Poynting vector distribution. The occurrence of the abnormal phenomenon depends on both hollow depth and width. The abnormal phenomenon takes place for smaller hollow depths, and there exists a critical hollow depth value, which changes with the hollow width. The abnormal phenomenon favors not only practical applications of TJ but also an in-depth understanding of the mechanism of its generation in a reflection mode.

Acknowledgements

Project supported by the National Natural Science Foundation of China (Grant No. 61875148), the Key Awards Program of Cultivating Outstanding Innovative Postgraduates in Arts and Sciences of Tianjin University (Grant No. C1-2022-002), the Talent Project of Anhui Science and Technology University (Grant No. DQYJ202304), the University-Level Research Project of Tianjin Sino–German University of Applied Sciences (Grant No. zdkt2018-007), China Association for Science and Technology Young Talent Support Project Doctoral Special Program, and the National High-level University Scholarship Program for Graduate Students of China Scholarship Council (Grant No. 202406250166).

References

[1] Liu Y Y, Liu X C, Li L, Chen W D, Chen Y, Huang Y R and Xie Z W 2017 *Chin. Phy. B* **26** 114201
[2] Gu G Q, Zhang P, Chen S, Zhang Y and Yang H 2021 *Photon. Res.* **9** 1157
[3] Yang Y J, Hua P R and Zhang D L 2022 *Chin. Phys. B* **31** 034201
[4] Li Y C, Liu X S, Xu X H, Xin H B, Zhang Y and Li B J 2019 *Adv. Funct. Mater.* **29** 1905568
[5] Yang H, Cornaglia M and Gijs M A 2015 *Nano Lett.* **15** 1730
[6] Gu G Q, Song J, Chen M, Peng X, Liang H D and Qu J L 2018 *Nanoscale* **10** 14182
[7] Yang Y J, Zhang D L and Hua P R 2022 *Results Phys.* **38** 105616
[8] Minin I V, Minin O V, Pacheco-Pena V and Beruete M 2015 *Opt. Lett.* **40** 2329
[9] Minin I V, Geints Y E, Zemlyanov A A and Minin I V 2020 *Opt. Express* **28** 22690
[10] Minin I V, Minin O V, Pacheco-Peña V and Beruete M 2016 *Quantum Electron* **46** 555
[11] Yue L Y, Yan B, Monks J N, Dhama R, Wang Z B, Minin O V and Minin I V 2018 *Ann. Phys-Berlin* **530** 1800032
[12] Minin I V, Liu C Y, Yang Y C, Staliunas K and Minin O V 2020 *Sci. Rep.* **10** 8459
[13] Yang Y J and Zhang D L 2024 *J. Opt. Soc. Am. B* **41** 1018
[14] Yang Y J, Yang B R, Zhang D L and Yuan N 2025 *Opt. Laser Technol.* **180** 111467
[15] Yang Y J, Zhang D L, Xue S D and Yuan N 2024 *Opt. Express* **32** 26374
[16] Yang Y J, Yang B R, Yuan M Q, Zhang D L, Yuan N and Xue S D 2025 *Measurement* **239** 115530
[17] Wang M, Yan Y, Mi Y and Jiang Y 2022 *J. Raman. Spectrosc.* **53** 1238
[18] Wang J, Yang S, Cao Y and Ye Y H 2022 *J. Phys. Chem. C* **126** 7542
[19] Sergeev A and Sergeeva K 2020 *Opt. Mater.* **110** 110503
[20] Dholakia K and Cižmár T 2011 *Nat. Photon.* **5** 335
[21] Winnewisser C and Lewen F and Helm H 1998 *Appl. Phys. A* **66** 593
[22] Geints Y E, Minin I V and Minin O V 2022 *Opt. Lett.* **47** 1786
[23] Geints Y E, Minin I V and Minin O V 2022 *Opt. Commun.* **524** 128779